Fabrication of α-FeSi₂ nanowhiskers and nanoblades *via* electron beam physical vapor deposition

Wenting Huang [a,b], Vesna Srot [c], Julia Wagner [d], Gunther Richter [b,*]

[a] *Institute for Applied Materials, Karlsruhe Institute of Technology, Hermann-von-Helmholtz-Platz 1, 76344 Eggenstein-Leopoldshafen, Germany*
[b] *Max Planck Institute for Intelligent Systems, Heisenbergstr. 3, 70569 Stuttgart, Germany*
[c] *Center for Electron Microscopy, Max Planck Institute for Solid State Research, Heisenbergstr. 1, 70569 Stuttgart, Germany*
[d] *Karlsruhe Nano Micro Facility (KNMF), Karlsruhe Institute of Technology, Hermann-von-Helmholtz-Platz 1, 76344 Eggenstein-Leopoldshafen, Germany*

HIGHLIGHTS

- α-FeSi₂ whiskers are grown at 900 °C on TiC/Si(100) by evaporation of Fe.
- Whiskers are freestanding and defect-free; surface facets are {100} planes.
- Fe adatoms and Si bulk atoms interdiffuse at the interface yielding α-FeSi₂.
- Not thermodynamic equilibrium defines the geometrical shape, but kinetic process.

GRAPHICAL ABSTRACT
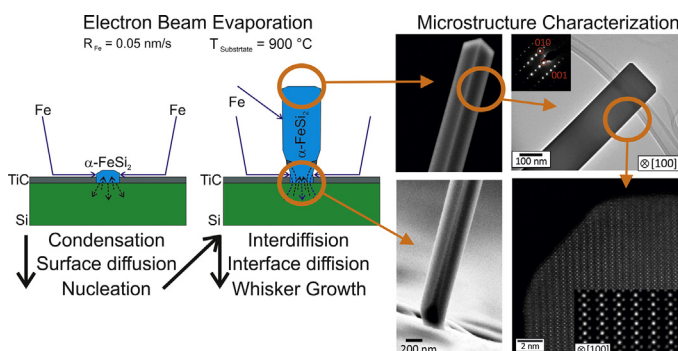
ABSTRACT

Iron disilicide nanowhiskers and nanoblades are synthesized by depositing Fe onto Si(100) substrates at about 900 °C *via* electron beam physical vapor deposition. The nanostructures are determined as single crystalline α-FeSi₂ with tetragonal lattice. The nanostructures are stable with prolong exposure under ambient condition, and no transformation towards β-FeSi₂ is detected after 2 h annealing at 500 °C and 800 °C under high vacuum condition (10^{-6} mbar). The growth directions of the whiskers are found as either [001] or [100]. However, in the blades we observe grow only in [100] crystallographic direction. Changing cross-sectional shape of the α-FeSi₂ whiskers from octagon at the root to rectangle at the upper part is observed and believed to be a result of the thermodynamic and kinetic anisotropy. SiO₂ layer formed on the surface of the structures because of its lower surface energy compared to all iron oxides. By this passivation, which prevents further oxidization, of the nanowhiskers is achieved. The α-FeSi₂ whiskers form by root growth.

1. Introduction

The Gibbs energy determines the geometrical shape of crystals: $\sum \gamma_{hkl} A_{hkl} = min$; the total of the surface energies is minimum under the constraint that the volume is constant. Typically, no knowledge on the mechanisms, which lead to the formation of this particular shape,

* Corresponding author.
E-mail address: richter@is.mpg.de (G. Richter).

can be derived from this basic thermodynamic consideration. Thus, predicting geometrical shapes of growing crystals *e.g.* for nanostructures or thin films is only possible if the kinetics of the particular growth process are understood. This is especially important if the typical equiaxed geometry of crystals is broken, because one or more dimension of the growing structure dominates. This results in one- or two-dimensional or structures, which are highly desired in modern technology. It is worth to remember and to point out that those surface facets that are attributed to high growth velocities vanish when the thermodynamic equilibrium is approached [1]. This already gives an indication that for the design of novel structures not only thermodynamic but also kinetic processed have to be considered. Kinetics processes are directly correlated with diffusion processes. Therefore is it important to tailor microstructures to guide diffusion. One way to do so is to use interfaces as preferred diffusion paths, leading to the formation of novel structures [2,3].

Silicides have attracted growing attention in the development of Si-based microelectronic industry, because of their good electrical conductivity and chemically and structurally stable silicide/silicon interface [4–7]. Iron disilicide is one of the promising candidates for thermoelectric and optoelectronic device applications [8]. According to the iron silicon phase diagram iron disilicide shows two kinds of crystal structures: α-FeSi$_2$ and β-FeSi$_2$ [9]. Most of the research efforts have been devoted to the orthorhombic β-FeSi$_2$ phase (Cmca) because of its semiconductor nature. Its direct band gap is $\approx$0.85 eV and optical absorption coefficient >10^{-5} cm^{-1} [10–13]. The β-FeSi$_2$ is stoichiometric and thermodynamically stable under ambient condition. The lack of research on the metallic α-FeSi$_2$ phase is probably because of the instability of the structure at room temperature. The α-FeSi$_2$ phase with tetragonal crystal structure (P4/mmm) is thermodynamically stable at temperatures above 950 °C [13,14] The metastable α-FeSi$_2$ at room temperature can be obtained by rapid cooling [15], or by ion-beam-induced epitaxial crystallization [16,17], or as precipitates [18,19]. The α-FeSi$_2$ was also reported as the phase at the early stage of epitaxial growth (<10 nm thick layers) [20,21], as the lattice mismatch between the Si(100) substrate (a = 0.543 nm) and α-FeSi$_2$ (a = b = 0.269 nm, c = 0.513 nm) is only about 0.9% along a or b axis. In contrast, it is about 1.45% and 2% for the β-FeSi$_2$ {101} and {110} planes (a = 0.986 nm, b = 0.779 nm, c = 0.783 nm) when epitaxially grown on the (110) Si substrate [22]. Upon cooling or annealing, or by increasing the thickness of the thin film, the α-FeSi$_2$ phase tends to relax into β-FeSi$_2$ phase [20,23]. The existence of vacancies in Fe sublattice in the α-FeSi$_2$ allows a rather wide range of the composition (poorer in Fe than β-FeSi$_2$) [24]. The metallic α-FeSi$_2$ with good electrical conductivity [23] is expected to play an important role in the integrated circuits, for example as Schottky barriers, ohmic contacts, and interconnects [25]. Moreover, α-FeSi$_2$ nano-stripes exhibit superparamagnetism at room temperature, which indicates the potential application in high-density magnetic memory storage and spintronics devices [26]. Low dimensional nanostructures have the prospect to act as model systems for future nanotechnology. Therefore, nanowire is perhaps one of the most studied nanomaterials in the past decade [27–29]. Most of the nanowires being studied today are semiconductor nanowires. They are compatible with the booming microelectronics industry and have already shown promising properties in other domains such as optoelectronics and biosensors [26,30,31]. The growth mechanism of one-dimensional structures, nanowires or whiskers, are not fully established. There are experimental observations for tip growth [32–34] but also for root growth [35–37]. Therefore, for each whisker system the growth conditions and the relevant atom incorporation site have to be deduced.

The present study reports the synthesis of metallic α-FeSi$_2$ nanostructures, including nanowhiskers and nanoblades *via* electron beam physical vapor deposition (EB-PVD) method at 900 °C. As a substrate Si(100) was used, which was coated with 35 nm TiC by magnetron sputtering. All the nanowhiskers and nanoblades were single crystalline and free-standing on the TiC/Si(100) substrate surface. The α-FeSi$_2$

structures were stable against aging under ambient condition, and no phase transition from α-FeSi$_2$ to β-FeSi$_2$ was observed after annealing for 2 h, at 500 °C and 800 °C, respectively. No structural one- or two-dimensional defects were observed in the whiskers or the blades. Thus, those perfect single crystalline nanoobjects are ideal for the research on the genuine material properties as function of dimensions. We demonstrate in our discussion the importance of interface and surface diffusion on the formation of nanostructures.

2. Experimental methods

Firstly the Si(100) substrates were cleaned in ultrasonic bath (acetone and isopropanol) before being transferred into a home built high vacuum (HV) system (base pressure $\approx 10^{-6}$ mbar). 10 min Ar-plasma cleaning with power of 100 W and $p_{Ar} = 1 \cdot 10^{-3}$ mbar was applied to remove the native oxide layers from the substrate surface. A 25–30 nm TiC layer was then deposited onto the substrate surface by magnetron sputtering at room temperature. TiC was acting in this case as the mediating layer, providing energy and probably structural heterogeneity on the substrate surface for the aggregation of Fe atoms. The deposition of Fe was carried out in an ultra-high vacuum (UHV) Molecular Beam Epitaxy (MBE, DCA Instruments, Finland) system with a base pressure of under 2×10^{-10} mbar. Fe was evaporated from an electron beam evaporator (MBE Komponenten, Germany). An elevated substrate temperature is required to facilitate surface diffusion, which is critical for the nucleation and subsequent growth of whiskers. In this work, the typical substrate temperatures applied were $T_S = 900$ °C. Fe deposition rate was chosen as $R = 0.05$ nm/s and was monitored with a quartz balance. Rotation of the specimen plate around its surface normal was applied during the entire processes in order to improve the homogeneity of the deposition.

After the deposition, the specimens were slowly cooled down to room temperature and subsequently retrieved from the UHV system for further *ex-situ* analysis. This latter involved microstructure investigations with scanning electron microscope (SEM) (LEO 1530VP Gemini) and transmission electron microscope (TEM) (Philips CM200 and JEOL ARM1250). Chemical analysis was carried out by HAADF-STEM imaging combined with EELS by using advanced TEM/STEM (JEOL ARM200F, JEOL Co. Ltd) microscope equipped with a cold field emission gun and a DCOR probe Cs-corrector (CEOS Co. Ltd). 3-dimensional atom probe tomography (ATP) analysis was done in a LEAP 4000XHR in Voltage mode with a pulse rate of 200 kHz, pulse fraction: 20%. The tip was cooled to 55.4 K.

For the TEM sample preparation, nanostructures (mostly whiskers) were collected by scratching the coated substrate surface with a standard 300-mesh TEM grid, covered with lacy or holey carbon film. Lamellae specimens of the cross-section of the whiskers were prepared by FIB (FEI Dual-Beam), which granted insights to the cross-sectional microstructures and to the growth mechanism. For lamellae TEM preparation, the whiskers were scratched onto a sacrificial Si wafer for support.

Annealing was carried out in two ways: the temperature was maintained at 500 °C for 1 h during cooling down in the MBE after deposition, or heating up to 500 °C and 800 °C and maintained for 2 h with a heating stage in TEM, with base pressure of about 10^{-6} mbar.

3. Results and discussion

Various structures were found on the TiC/Si substrate surface after the Fe deposition at about 900 °C. Fig. 1 shows SEM images of 2 whiskers (a, b) and 2 blades (c, d). The whiskers and blades are defined here by the different aspect ratio of the cross-sections. The cross-sectional shape of the whiskers was close to a square (the cross sectional aspect ratio is usually <2:1), with width varied from 40 to 300 nm. While that of the blades was an elongated rectangle (aspect ratio of the cross sectional shape is often higher than 5:1), with thickness in the range similar to the whiskers (40–300 nm), and the width of about 500 nm–
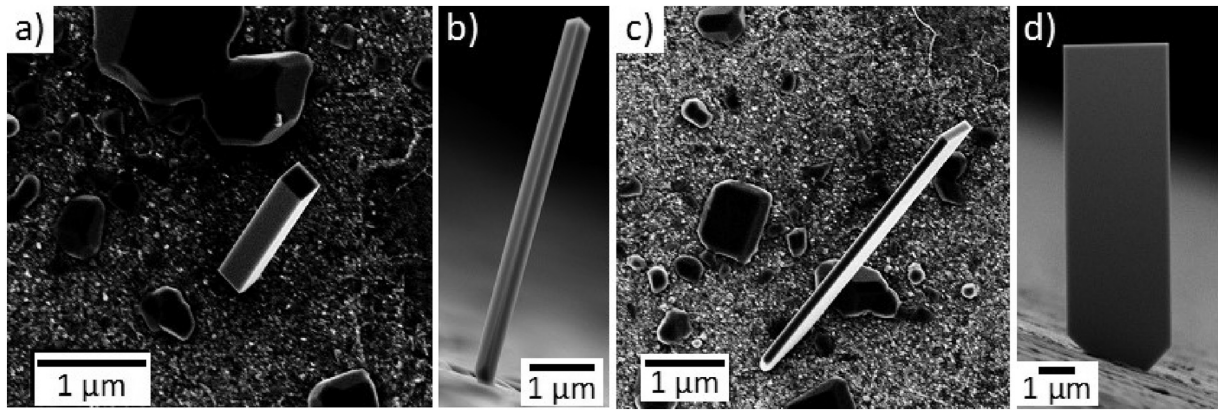
Fig. 1. SEM micrographs of 2 FeSi$_2$ whiskers (a, b) and 2 FeSi$_2$ blades (c, d) grew on a Si(100) substrate after the deposition of 180 nm (nominal value) of Fe at 900 °C.

5 μm. Both whiskers and blades were about several micrometers long (usually longer than 10 μm). Generally, there is no taper observed neither in the blades nor for the whiskers, only close to the substrate deviations from the prismatic shape can be found. The surface facets seem to be smooth and to be devoid of big surface steps. There are also particles/ islands with equiaxed geometry observed on the substrate surface with random shape, which were usually polycrystalline; those were not studied in details within this paper.

The crystallography of the iron silicide structures was studied with electron diffraction. Fig. 2-a and -b show the TEM bright-field (BF) images of an iron silicide whisker. The corresponding diffraction patterns in the insets match tetragonal structure of the α-FeSi$_2$ with lattice parameters of $a = b = 0.269$ nm, $c = 0.513$ nm. No taper could be seen in nanowhiskers, projected width of the nanostructure in side view shows the same value at the tip and the root region. Only at the very

root region close to the substrate a smaller diameter of the whisker is observed. The contrast was homogeneous throughout the entire whisker for the BF image taken from zone axis [100]. Again, indicating that also in projection the thickness is not changing. Additionally no one-dimensional defects, *e.g.* dislocations, or two-dimensional defects, *e.g.* grain boundaries, were detected in any of the investigated nanostructures.

Tilting the same structure by 45° around the whisker axis enabled the recording of a BF image taken from zone axis [110] (Fig. 2-b). Thickness fringes were observed in the direction parallel to the whisker axis. The fringes were symmetrical with respect to the central axis of the whisker. The above can be understood by taking into account the (almost) square shaped cross-section of the whiskers observed in Fig. 2-a. No contrast variation shall be observed when the incident beam is perpendicular to two of the four sides (Fig. 2-c) since the prismatic
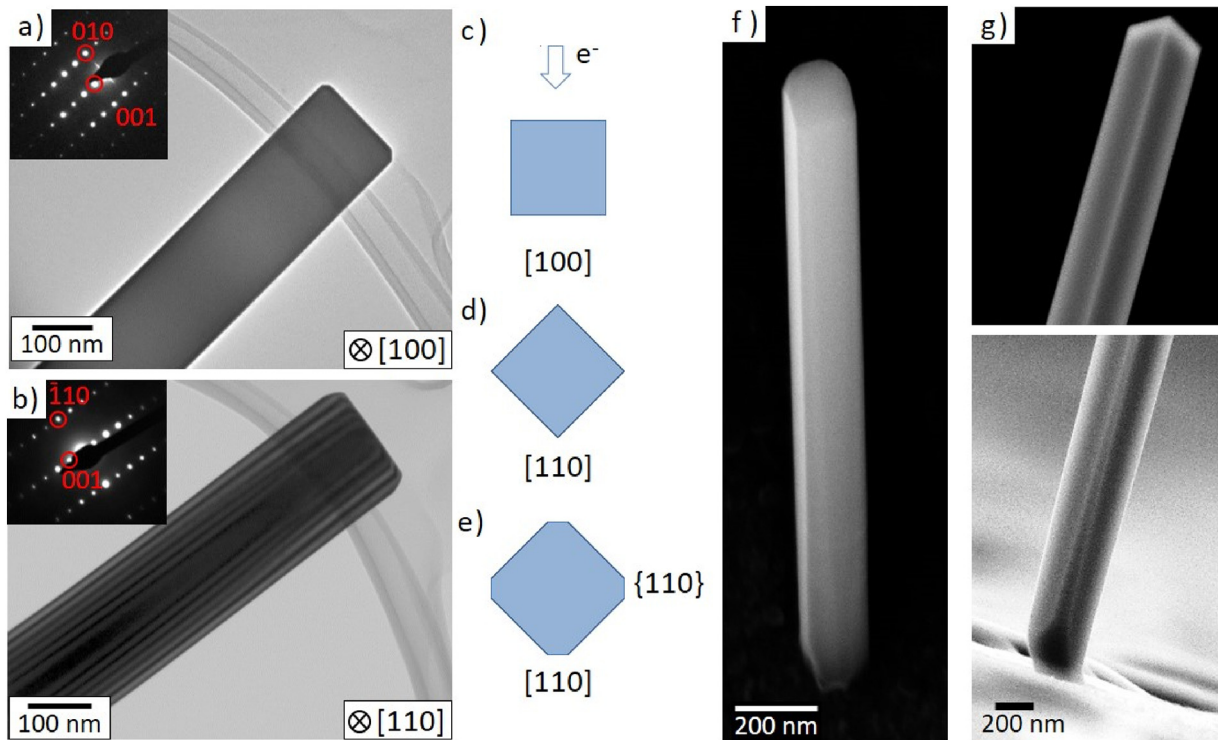
Fig. 2. TEM BF micrographs of a FeSi$_2$ whisker from zone axes (a) [100] and (b) [110]. The insets are the corresponding diffraction patterns. The diffraction direction of whisker axis is indexed as [001] in red circles, the diffraction directions perpendicular to the zone axis and whisker axis are also indexed respectively. (c) and (d) Schematic representations of the transmission geometry to obtain micrograph a and b, respectively. (e) Schematic representation of the cross-section of a FeSi$_2$ whisker with truncated facets. (f, g) SEM micrograph of two FeSi$_2$ whisker showing the transition of its cross-sectional area from octagon at the root to square at the tip. (For interpretation of the references to color in this figure legend, the reader is referred to the web version of this article.)

body is not tapered. On the other hand, if the incident beam was aligned with one of the diagonals (Fig. 2-d), contrast variations would appear due to changes in the projected thickness of the whisker. This is due the dynamical diffraction condition and the well-defined microstructure of the whiskers. The analysis further implies that the sidewalls of the whiskers were composed of 4 crystal planes of the {100} family.

Extra facets were sometimes observed near the root of the $FeSi_2$ whiskers (Fig. 2-f, g), mostly on thicker and shorter whiskers. With whisker axis of ⟨001⟩ crystallographic direction, these facets appearing at the junction were considered to be low index {110} planes (Fig. 2-e), to form geometrically 45° with two adjacent {100} sidewalls. This can be further supported by thermodynamic consideration, as these crystal planes have relatively low surface energy. However, it is entirely possible that these small facets were also present on the whisker shown in Fig. 2-a and -b, despite not being visible due to the peculiarity of the transmission technique. The appearance of the {110} planes at the root part of the whiskers, or to rephrase in a more correct way, the

disappearance of the {110} planes other than at the root part of the whiskers, is understood as of both, thermodynamic and kinetic origins. The details will be discussed in following parts.

Fig. 3 shows the BF-TEM, high-resolution TEM (HRTEM) and high-angle annular dark-field (HAADF) scanning TEM (STEM) images of two cross-sectional lamellae cut from two different $FeSi_2$ whiskers. The lamella's normal is parallel to the whisker geometrical axis. The two cross-sections differ very much in size (50×90 nm^2 for the one shown in Fig. 3-a and 140×220 nm^2 for the one in Fig. 3-c), despite having a similar aspect ratio (1.8:1 and 1.6:1, respectively). Fig. 3-a and -c depict the BF images taken along the whisker axis. Again no defects were visible in the specimens. The slight contrast change can be attributed to beam damage from the STEM imaging process. Despite the change in absolute size, the surface facets of both whiskers are atomically flat. No surface steps on the facets can be observed. This is in full agreement with the SEM studies. The sacrificial Si crystal is seen in left side of the micrographs. The whisker rest on a low index surface plane
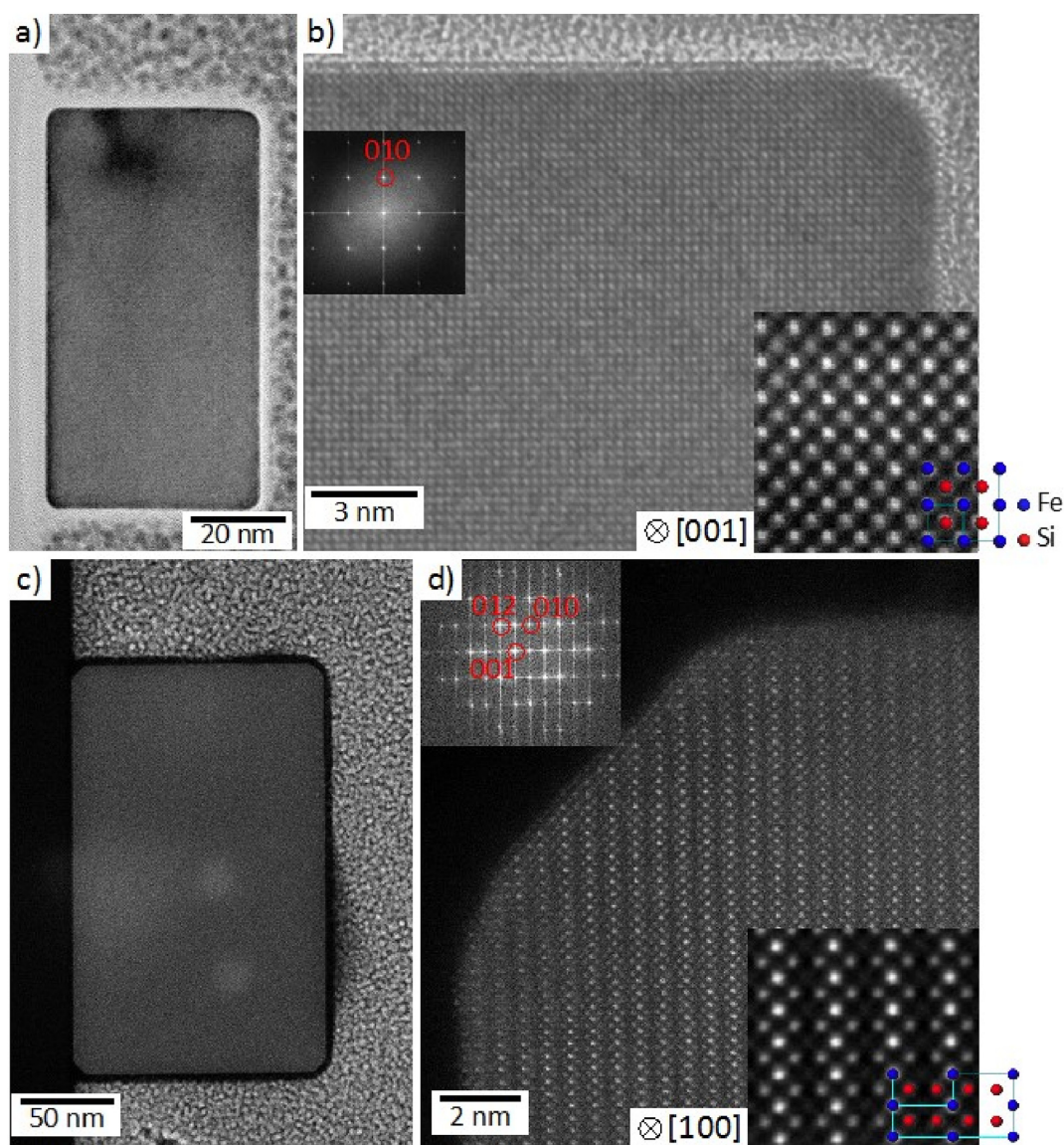
Fig. 3. (a) TEM micrograph taken along the whisker axis, (b) HRTEM image, the corresponding FFT pattern (inset i) and ABSF filtered HAADF-STEM image (inset ii) of the cross-section of a $FeSi_2$ whisker grown along the [001] direction. (c) Low magnification HAADF-STEM micrograph, (d) HAADF-STEM image, the corresponding FFT pattern (inset iii) and ABSF filtered HAADF-STEM image (inset iv) of the cross-section of another $FeSi_2$ whisker grown along the [100] direction. The schematics of the α-$FeSi_2$ lattice are shown in the bottom-right corner of the HAADF images. The blue spheres are Fe atoms and the red ones are Si atoms. In (a) and (c) the Si support is seen on the left side. (For interpretation of the references to color in this figure legend, the reader is referred to the web version of this article.)

on the surface of the sacrificial Si crystal after scratching. The insets i and iii in Fig. 3-b and -d are fast Fourier transform (FFT) calculated from the real space images. In first approximation they can be interpreted similar to electron diffraction patterns. The HAADF real space image and the FFT patterns show clearly that the crystallographic orientations of the two whiskers were also different. The FFT pattern of the first sample (Fig. 3-b, inset i) indicates that the axial direction of the whisker (i.e., the normal of the cross-sectional plane) was along the [001] direction and that its four sidewalls were all constructed with {010} planes. This is consistent with what we have previously observed on the other sample (Fig. 2). The FFT pattern of the second sample (Fig. 3-d, inset iii), however, was surprisingly different. The pattern fits well with what was expected from the [100] zone axis of tetragonal α-FeSi$_2$. The growth direction of the whisker in this case was the [100] direction with its sidewalls consisting of 2 {010} and 2 {001} planes.

The different atom arrangement in the two samples can also be observed in the HAADF images. For the insets ii and iv in Fig. 3-b and -d, an average background subtraction filter (ABSF) was applied to help better visualize the chemical contrast. The brighter spots are the heavier element, which in this case are the Fe atoms. The two HAADF images agree well with the schematic atomic structure of α-FeSi$_2$ viewed from zone axis [001] and [100] respectively. Careful inspection of the atomic structure did not reveal any defects parallel to the whisker axis. Especially no dislocation line was found in the whisker.

Finally, the two whiskers also showed a difference on how adjacent surface facets of the prismatic body were joined (Fig. 3-a and -c). A round edge was observed on the smaller cross-section where two {010} facets met (Fig. 3-b). No low indexed surface facet can be identified for the corner area. This phenomenon is in agreement with the configurational entropy concept for high indexed surface facets at elevated temperatures [38,39], where an increase of disorder and by this an increase of the entropy reduces the surface energy at crystal edges and therefore leads to round corners compared to ideal sharp edges. In contrast, for the cross-section of the larger whisker (Fig. 3-d) a small crystal plane, indexed as the {012} plane, was observed at the junction between the {010} and the {001} facet. However, close inspection for the edges between the three facets reveal again a round, blunt individual edges.

The axial growth direction of [100] was also found in a α-FeSi$_2$ blade, as shown in Fig. 4. Its width is about 950 nm, much larger than the diameter of the whiskers. From the electron diffraction pattern (Fig. 4-b), the axial direction of the blade was identified as parallel to the [100] crystallographic direction. Its two largest surfaces are from the {001} family. Again the BF-TEM micrograph does not indicate the presence of any crystal defect.

In summary, it is worth mentioning, that except the thickness contrast (Fig. 2-b), we observed no contrast of edge dislocations, crew dislocations, stacking faults, grain boundaries, and second phase from the BF-TEM (Fig. 2), HRTEM, HAADF-STEM (Fig. 3) analyses. In addition, all the whiskers and blades were perfect single crystals with well-
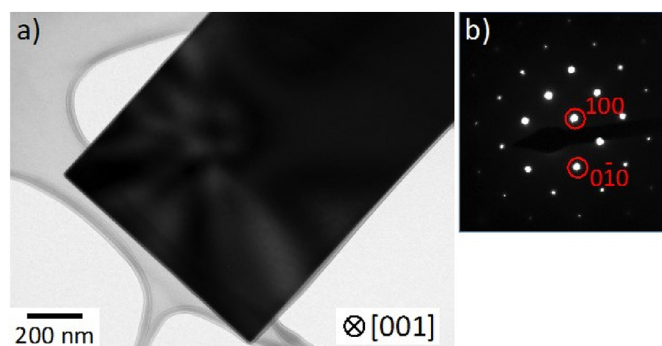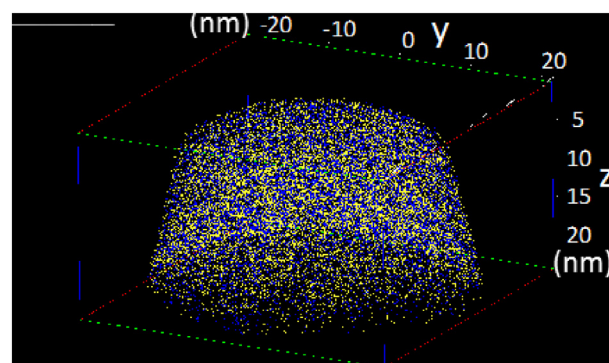
Fig. 5. 3-dimensional atom probe tomographic reconstruction of part of a FeSi$_2$ whisker. Blue counts came from Fe, yellow counts were Si. (For interpretation of the references to color in this figure legend, the reader is referred to the web version of this article.)

defined surface facets, which made them ideal for the research on the material properties without the effects of the defects.

APT analysis (Fig. 5) revealed the homogeneous chemical composition at the center of the iron silicide whiskers as atomic percentage of 65.88 ± 0.03 at.% Si and 33.96 ± 0.03 at.% Fe, with ratio of Fe:Si = 1:2 (Table 1). The 0.16 ± 0.03 at.% Ga counts were introduced from the focused ion beam (FIB) during sample preparation. No other elements could be detected in the analysis within the detection limit, showing that apart the Ga introduction during sample preparation, only Si and Fe are present in the nanowhiskers. Due to the sample preparation of the tip, the APT measurements measured mostly the core part of the whisker. Therefore, the chemical composition of the FeSi$_2$ whisker (in Fig. 3-c) surface was further examined with electron energy loss spectroscopy (EELS) on a cross-section lamella. The pathway of the EELS linescan on the cross-section is marked by the yellow line in Fig. 6-a. The background subtracted spectra were summed separately for those measured on the crystallized core (red rectangle) and those on the amorphous shell (green rectangle). The result is shown in Fig. 6-b and -c for the data near the Si edge and near the O/Fe edge, respectively. The fine structure details of Si-L$_{2,3}$ edges from core and shell areas appear different. Peak positions and fine structural details of Si-L$_{2,3}$ edges in core and shell spectra are in good agreement with spectra shown for crystalline Si (99 eV) and SiO$_2$ (106.3 eV), respectively [40,41]. The relative reduction in intensity of the Fe peaks compared to the Si peaks on the shell (green) curve indicates, that the oxide layer at the surface of the FeSi$_2$ whiskers was mainly composed of SiO$_2$ with only a limited amount of oxides of iron. Indeed, the oxidation process of silicides usually proceeds by diffusing the Si atoms towards the surface and the metal atoms back into the bulk [42,43]. The formation of stable SiO$_2$ at the surface can easily prevent further oxidation of the whisker and the formation of oxides of iron.

The high aspect ratio of the whiskers is the result of kinetic anisotropy since the thermodynamic equilibrium structure has to resemble the Wulff shape, which is determined by the corresponding surface energies [44]. The growth of the whiskers occurs in both the axial (along the whisker axis) and the radial (perpendicular to the whisker axis) directions, albeit one (axial) much faster than the other (radial). Historically, the axial growth in whiskers was related to the existence of a screw dislocation, with its Burgers vector parallel to the whisker axis [45,46]. It was thought, that the point where the dislocation emerges

Fig. 4. (a) BF-TEM image and (b) corresponding diffraction pattern of a FeSi$_2$ blade.

Table 1
APT results on a FeSi$_2$ whisker.

	Counts	Average at.%
Si	308,724	65.88 ± 0.03
Fe	159,150	33.96 ± 0.03
Ga	754	0.16 ± 0.03
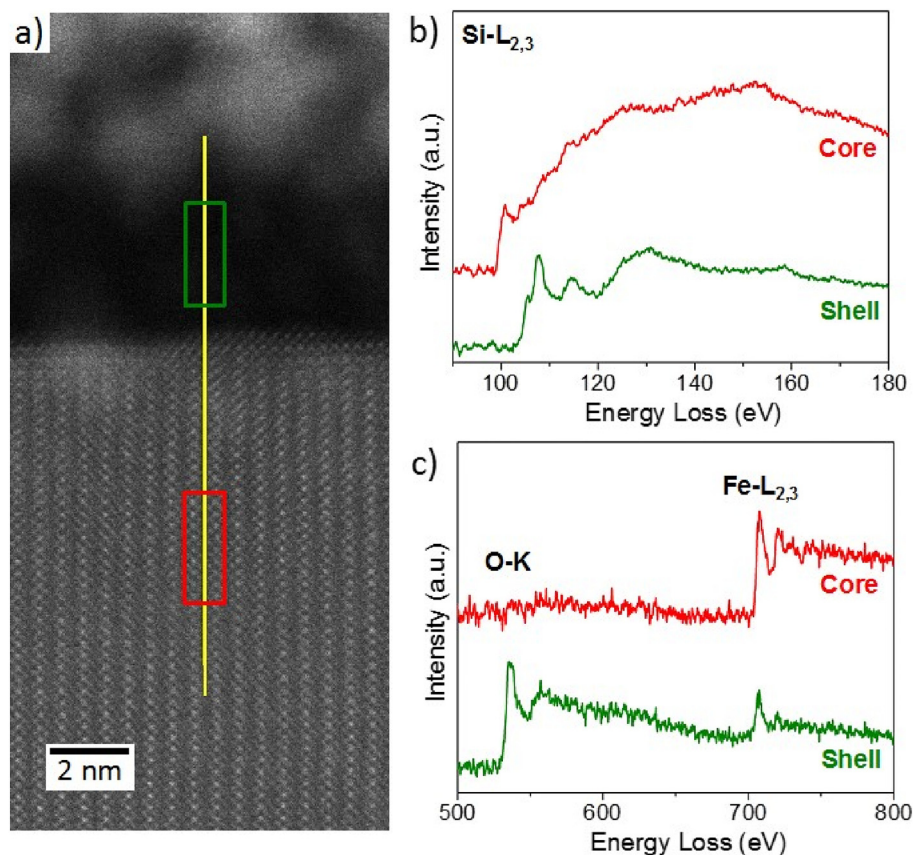
Fig. 6. (a) HAADF-STEM image of a cross-section lamella with marked position of EELS linescan. (b) Background subtracted EEL spectra of Si-$L_{2,3}$ edges. (c) Background subtracted EEL spectra of O-K and Fe-$L_{2,3}$ edges. The green (red) curve is the result summed on the area marked by the green (red) rectangle, for the shell (core) part of the structure. (For interpretation of the references to color in this figure legend, the reader is referred to the web version of this article.)

from the substrate and later from the tip of the whisker will act as preferred attachment site for the adatoms during deposition. By this the symmetry of the Wulff shaped nucleus is broken and a whisker is formed [46]. Since the FeSi$_2$ whiskers are dislocation free, this model does not support α-FeSi$_2$ whisker growth. Therefore, the mechanism how the symmetry is broken is still elusive.

Fig. 7 shows our hypothesis of the α-FeSi$_2$ whisker formation. The TiC layer is necessary for the nanowhisker growth, without only islands form on the surface. We speculate, that the TiC layer is not homogeneous in thickness, and even might have small parts of the Si not covered forming holes. The nucleation rate in thin film growth is mainly governed by the activation energies of diffusion and adsorption [47]. If those energies are not invariant to translation, sites with higher nucleation rate will form the first nuclei. Then, subsequently random, statistical nucleation is followed on homogeneous substrate surface areas. The later nucleation leads to the growth of equiaxed island/particles.

Whereas initially, probably at in the assumed holes, the whiskers and blades are nucleated. Therefore, the first function of the TiC layer is, to provide preferred nucleation sites for whisker growth, indicated as a hole in Fig. 7-a. Secondly, it allows for enhanced surface diffusion compared to the pure Si(100) surface. Both are functions are similar to the thin C layer for the growth on Au, Ag or Cu nanowhiskers [48].

The nucleation site has to allow for outward diffusion of Si and the formation of a α-FeSi$_2$ nucleus (Fig. 7-b). In co-evaporation experiments, it was speculated, that the formation of α-FeSi$_2$ or β-FeSi$_2$ seem to depend on the nucleation site [49]. No craters or depressions are observed around the nanowhiskers roots indicating that the fluxes of Fe and Si across the interface are similar. The diffusivity of Fe in Si, Si in Fe and the self-diffusion of Fe can be estimated for the applied substrate temperature [50–52]. According to the estimation, the diffusion of Fe in Si is the fastest followed by the Si diffusion in Fe and the self-diffusion of Fe. The latter ratio is due to the smaller atom size of Si and
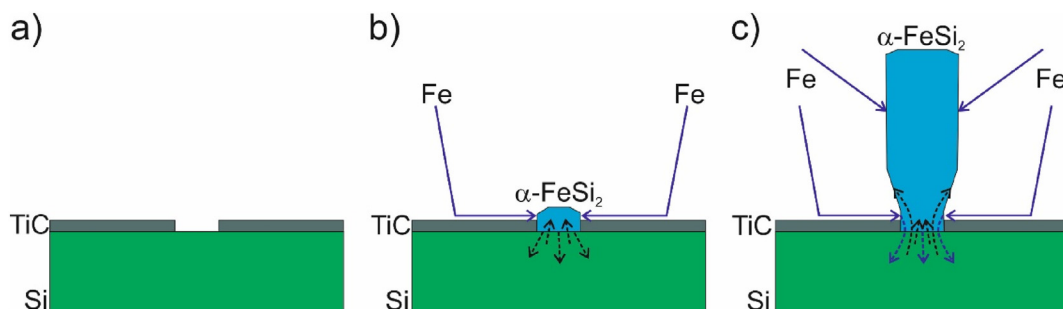
Fig. 7. Schematic of proposed α-FeSi$_2$ whisker growth. (a) Surface prior Fe deposition. (b) Condensation and surface diffusion of Fe (solid arrow): preferred nucleation of FeSi$_2$ in inhomogeneity of TiC layer; interdiffusion of Fe and Si (dashed arrows). (c) Axial growth of whisker: diffusion of Fe and Si towards interface and α-FeSi$_2$ formation at interface.

the hindering of diffusion by the ferromagnetic ordering of Fe [53]. In addition, it is argued that, the interstitial diffusion mechanism of Fe in Si is faster since it does not rely on intrinsic point defects in the matrix crystal [54]. The formation of α-FeSi$_2$ phase was possibly preferred by the interface as the mismatch of the structure with Si substrate is smaller than β-FeSi$_2$. The lower strain energy stabilized the structure [16,20,55]. The reaction started with the interstitial diffusion of Fe atoms into the Si lattice. This increased the neighboring atoms of Si atoms, and weakened the covalent bonds of Si atoms. The interstitials concentration would be much higher than that in the lattice, therefore Si atoms at the interface can be removed from the Si lattice [56]. Moreover, the interstitial diffusion of Fe atoms into Si lattice would leave behind a high density of vacancies at the interface. The exact atomic structure and composition of the α-FeSi$_2$/Si(100) interfaces however remains unclear for α-FeSi$_2$ whisker growth. There are reports for epitaxial growth of α-FeSi$_2$ on Si(100) [20,21], however also other interface orientations allow for α-FeSi$_2$ formation on Si(111) [49]. In the second case, β-FeSi$_2$ islands forms an epitaxial orientation relationship with Si. Whereas α-FeSi$_2$ has an abrupt interface but the (001) plane has an inclination of ~10° to the Si(111) surface [49]. Such an inclined interface orientation is expected to have a higher defect or vacancy density compared to an epitaxial one [57]. The high vacancy density in and close to the interface has two effects: (i) further enhancement of the diffusion of Si atoms from the substrate lattice into whiskers by exchanging positions with vacancies and (ii) providing an effective diffusion path for Fe atoms in the interface.

After the nucleation of α-FeSi$_2$ islands, the axial and radial growth of the whiskers has to be considered (Fig. 7-c), Ruth and Hirth [58] studied the sources of adatoms contributing to the axial growth of whiskers. Following their arguments, the source of Fe adatoms is twofold: Fe atoms condensate from the vapor phase either on the substrate surface and then diffuse to the whisker or impinge direct on the side facets of the whisker. Then adatoms from both sources diffuse to the incorporation site and contribute to the axial growth. In contrast, the source of the Si atoms contributing to the α-FeSi$_2$ whisker formation has only one source, it can only be the volume of the Si(100) substrate close to its surface. Therefore, the axial growth of the whisker was mostly attributed to the aggregation of Fe adatoms and diffusion of Si atoms in the whisker-substrate interface. Since the growth occurs at the whisker-substrate interface, it is called root growth mode. The incorporation of Fe adatoms in the interface and the Silicide formation is kinetically much more effective compare to the radial growth process, resulting in the one-dimensional growth of the whiskers. Radial growth can only occur by secondary nucleation on the side facets by the condensation and diffusion of Fe adatoms on the whisker sidewalls together with the diffusion of Si atoms towards the whisker surface. The freshly grown part near the root of the whisker (root growth) has the equilibrium cross-sectional shape of an octagon (truncated square shaped cross-section with large {010} and small {110} facets). Nucleation of a new FeSi$_2$ layer on the {110} facets has a higher rate, therefore the four {110} facets have a faster kinetic growth velocity [59] and vanish with the extensive radial growth, resulting in a square cross section, as demonstrated in Fig. 2. Since the α-FeSi$_2$ whiskers grow in root growth mode, the octagon cross section is only seen on the fresh grown part (root) of the whiskers.

The transition temperature from the low-temperature phase β-FeSi$_2$ to the high-temperature phase α-FeSi$_2$ is at approximately 950 °C, which is higher than the substrate temperature (900 °C) during deposition. The α-FeSi$_2$ structures were found to be stable at elevated temperature. After annealing at 500 °C, and 800 °C for 2 h, no change on crystal structure was observed under electron diffractions. The tetragonal crystal structure was retained after two years aging under ambient condition, even no further oxidation was detected. The stabilization mechanism is speculated as attributed from factors: the deviation of chemical composition from stoichiometry could be one of the reasons, as the orthorhombic lattice of β-FeSi$_2$ requires more Fe atoms; The α-

FeSi$_2$ to β-FeSi$_2$ phase transformation was probably also suppressed by geometrical constrain of the high aspect ratio structures and the high surface to volume ratio with high surface stress.

4. Conclusion

We have successfully synthesized α-FeSi$_2$ nanowhiskers and nanoblades on Si(100) substrate at about 900 °C. The crystal structures and the chemical composition of the nanostructures were studied. Both whisker and blade structures were defect-free single crystals with tetragonal lattice. There were two possible growth directions of the whiskers, either [001] or [100]. But only [100] growth axis was observed on the blades. The change of cross sectional shape of the α-FeSi$_2$ whiskers from octagon at the root to rectangle at the upper part was credited to the thermodynamic and kinetic anisotropy. It also indicated the root as the incorporation site for the whisker growth. The structures were covered by a layer mainly of SiO$_2$ because of the lower surface energy than the iron oxides, which then passivated the further oxidation of the rest part of whiskers. All the tetragonal α-FeSi$_2$ structures were stable up to 800 °C, and were stable against aging and oxidation under ambient condition.

We demonstrate in our result the importance knowledge of kinetics and diffusion on nanostructure formation. α-FeSi$_2$ whiskers only grow when the diffusion of Fe adatoms from the substrate surface and Si from the bulk to the interface is balanced. The special properties of the interface, the higher vacancy density in particular, allows for a continuous inward diffusion of the adatoms from the substrate leading to root growth. The cross-section is governed by the nucleation rate of new layers on the surface facets. Since that rate is also dependent on kinetic process and on the orientation of the surface facets, an almost square shaped cross-section can evolve during growth. An explanation by pure thermodynamic equilibrium concepts would not allow for whisker formation. To summarize, only by combining those fundamental kinetic processes allows for the synthesis of new unique structures. This is even more true for nanostructures, since surface and interface effects are compared to bulk properties dominant in such length scales.

CRediT authorship contribution statement

Wenting Huang: Conceptualization, Investigation, Validation, Writing - original draft, Writing - review & editing. **Vesna Srot:** Investigation. **Julia Wagner:** Investigation. **Gunther Richter:** Conceptualization, Supervision, Validation, Writing - original draft, Writing - review & editing.

Acknowledgements

References

[1] W. Kossel, Zur Theorie des Kristallwachstums, Nachrichten von der Gesellschaft der Wissenschaften zu Göttingen 1927, pp. 135–143.
[2] D. Amram, L. Klinger, N. Gazit, H. Gluska, E. Rabkin, Grain boundary grooving in thin films revisited: the role of interface diffusion, Acta Mat 69 (2014) 386–396.
[3] A. Kumar, H. Barda, L. Klinger, M.W. Finnis, V. Lordi, E. Rabkin, D.J. Srolovitz, Anomalous diffusion along metal/ceramic interfaces, Nature Com 9 (2018) 5251.
[4] P.A. Bennett, Zhian He, David J. Smith, F.M. Ross, Endotaxial silicide nanowires: a review, Thin Solid Films 519 (24) (2011) 8434–8440.
[5] M. Fedorov, Thermoelectric silicides: past, present and future, J. Thermoelectr. 2 (2009) 51–60.
[6] S. Chen, P. Yeh, W. Wu, U. Chen, Low resistivity metal silicide nanowires with extraordinarily high aspect ratio for future nanoelectronic devices, ACS Nano 5 (2011) 9202–9207.
[7] A.L. Schmitt, J.M. Higgins, J.R. Szczech, S. Jin, Synthesis and applications of metal silicide nanowires, J. Mater. Chem. 20 (2010) 223–235.

[8] D. Leong, M. Harry, K.J. Reeson, K.P. Homewood, A silicon/iron-disilicide light-emitting diode operating at a wavelength of 1.5 μm, Nature 387 (1997) 686–688.

[9] P. Franke, H.J. Seifert, Ternary Steel Syst. Phase Diagrams Phase Transit. Data, Springer, Berlin, Heidelberg, 2012 33.

[10] M.C. Bost, J.E. Mahan, Optical properties of semiconducting iron disilicide thin films, J. Appl. Phys. 58 (1985) 2696–2703.

[11] N. Kim, H. Kim, W. Lee, Optical and electrical properties of β−FeSi₂ single crystals, J. Korean Phys. Soc. 38 (2001) 803–805.

[12] Z. Yang, K.P. Homewood, M.S. Finney, M.A. Harry, K.J. Reeson, Optical absorption study of ion beam synthesized polycrystalline semiconducting FeSi₂, J. Appl. Phys. 78 (1995) 1958–1963.

[13] C.A. Dimitriadis, J.H. Werner, S. Logothetidis, M. Stutzmann, J. Weber, R. Nesper, Electronic properties of semiconducting FeSi₂ films, J. Appl. Phys. 68 (1990) 1726–1734.

[14] T.D. Hunt, K.J. Reeson, K.P. Homewood, S.W. Teon, R.M. Gwilliam, B.J. Sealy, Optical properties and phase transformations in α and β iron disilicide layers, Nucl. Instruments Methods Phys. Res. B 84 (1994) 168–171.

[15] U. Birkholz, J. Schelm, Mechanism of electrical conduction in β-FeSi₂, Phys. Status Solidi 27 (1968) 413–425.

[16] X.W. Lin, M. Behar, J. Desimoni, H. Bernas, J. Washburn, Z. Liliental-Weber, Low-temperature ion-induced epitaxial growth of α-FeSi2 and cubic FeSi in Si, Appl. Phys. Lett. 63 (1993) 105–107.

[17] R.L. Maltez, M. Behar, X.W. Lin, Ion-beam induced sequential epitaxy of α, β and γ-FeSi2 in Si (100) at 320 °C, Nucl. Instruments Methods Phys. Res. B 106 (1995) 400–403.

[18] A.G. Cullis, L.E. Katz, Electron microscope study of electrically active impurity precipitate defects in silicon, Philos. Mag. 30 (1974) 1419–1443.

[19] D.A. Ramappa, W.B. Henley, Stability of iron-silicide precipitates in silicon, J. Electrochem. Soc. 144 (1997) 4353–4356.

[20] J. Chevrier, P. Stocker, Epitaxial growth of α-FeSi2 on Si(111) at low temperature, EPL (Europhysics Letters) 22 (1993) 449–454.

[21] U. Starke, W. Weiss, M. Kutschera, R. Bandorf, K. Heinz, High quality iron silicide films by simultaneous deposition of iron and silicon on Si(111), J. Appl. Phys. 91 (2002) 6154–6161.

[22] N. Cherief, C. D'Anterroches, R.C. Cinti, T.A. Nguyen Tan, J. Derrien, Semiconducting silicide-silicon heterojunction elaboration by solid phase epitaxy, Appl. Phys. Lett. 55 (1989) 1671–1673.

[23] C. Kloc, E. Arushanov, M. Wendl, H. Hohl, U. Malang, E. Bucher, Preparation and properties of FeSi, α-FeSi₂ and β-FeSi₂ single crystals, J. Alloys Compd. 219 (1995) 93–96.

[24] F.A. Sidorenko, P.V. Geld, L.B. Dubrovskaya, Nature of the phase of the Fe-Si system, Fiz. Met. Met. 8 (1959) 735.

[25] S.P. Murarka, Silicide thin films and their applications in microelectronics, Intermetallics 3 (1995) 173–186.

[26] J.K. Tripathi, G. Markovich, I. Goldfarb, Self-ordered magnetic α-FeSi₂ nanostripeson Si(111), Appl. Phys. Lett. 102 (2013), 251604.

[27] A.R. Aliana, Y. Jub, S.A. Meguid, Comprehensive atomistic modeling of copper nanowires-based surface connectors, Mater. Des. 175 (2019), 107812.

[28] A. Kosinova, D. Wang, P. Schaaf, A. Sharmaa, L. Klinger, E. Rabkin, Whiskers growth in thin passivated Au films, Acta Mat 149 (2018) 154–163.

[29] J. Kou, A. Yu, Y. Liu, M. Jia, J. Guo, R. Wen, Y. Lei, Y. Zhu, Y. Zhang, J. Zhai, Piezotronics modulates high sensitivity relative humidity sensor based on single tellurium microwire, Semicond. Sci. Technol. 34 (2019), 075011.

[30] A. Balandin, K.L. Wang, Significant decrease of the lattice thermal conductivity due to phonon confinement in a free-standing semiconductor quantum well, Phys. Rev. B 58 (1998) 1544–1549.

[31] X.Y. Zhao, C.M. Wei, L. Yang, M.Y. Chou, Quantum confinement and electronic properties of silicon nanowires, Phys. Rev. Lett. 92 (2004), 236805.

[32] R.S. Wagner, W.C. Ellis, Appl. vapor-liquid-solid mechanism of single crystal growth, Phys. Lett. 4 (1964) 89–90.

[33] Y.-C. Chou, K. Hillerich, J. Tersoff, M.C. Reuter, K.A. Dick, F.M. Ross, Atomic-scale variability and control of III-V nanowire growth kinetics, Science 243 (2014) 281–284.

[34] J.D. Eshelby, A tentative theory of metallic whisker growth, Phys. Rev. 91 (3) (1953) 755–756.

[35] U. Lindborg, A model for the spontaneous growth of zinc, cadmium and tin whiskers, Acta Met 24 (2) (1976) 181–186.

[36] A.G. Nasibulin, S. Rackauskas, H. Jiang, Y. Tian, P.R. Mudimela, S.D. Shandakov, L.I. Nasibulina, S. Jani, E.I. Kauppine, Simple and rapid synthesis of α-Fe₂O₃ nanowires under ambient conditions, Nano Res. 2 (2009) 373–379.

[37] A. Kushima, K,P. So, C. Su, P. Bai, N. Kuriyama, T. Maebashi, Y. Fujiwara, M,Z. Bazant, J. Li, Liquid cell transmission electron microscopy observation of lithium metal growth and dissolution: root growth, dead lithium and lithium flotsams, Nano Energy 32 (2017) 271–279.

[38] J.W. Cahn, R. Kikuchi, Theory of domain walls in ordered structures—I. Properties at absolute zero, J. Phys. Chem. Solids 20 (1/2) (1961) 94–109.

[39] R. Kikuchi, J.W. Cahn, Theory of domain walls in ordered structures—II: pair approximation for nonzero temperatures, J. Phys. Chem. Solids 23 (1962) 137–151.

[40] L.A.J. Garvie, A.J. Craven, R. Brydson, Use of electron-energy loss near-edge fine structure in the study of minerals, Am. Mineral. 79 (1994) 411–425.

[41] R. Imlau, A. Kovács, E. Mehmedovic, P. Xu, A.A. Stewart, C. Leidinger, R.E. Dunin-Borkowski, G. Bihlmayer, H. Wiggers, R. Carius, U. Kolb, M. Luysberg, Structural and electronic properties of β-FeSi₂ nanoparticles: the role of stacking fault domains, Phys. Rev. B 89 (2014), 054104.

[42] H. Jiang, C.S. Petersson, M.-A. Nicolet, Thermal oxidation of transition metal silicides, Thin Solid Films 140 (1986) 115–130.

[43] L. Stolt, O. Thomas, F.M. D'Heurle, Oxidation of titanium, manganese, iron, and niobium silicides: marker experiments, J. Appl. Phys. 68 (1990) 5133–5139.

[44] G. Wulff, Frage der Geschwindigkeit des Wachsthums und der Auflösung der Krystallflächen, Zeitschrift für Krystallographie und Mineralogie 34 (1901) 449–530.

[45] G.W. Sears, A mechanism of whisker growth, Acta Met 3 (1955) 367–369.

[46] S.S. Brenner, G.W. Sears, Mechanism of whisker growth—III nature of growth sites, Acta Met 4 (1956) 268–270.

[47] D. Walton, T. Rhodin, R.W. Rollins, Nucleation of silver on sodium chloride, J. Chem. Phys. 38 (1963) 2698–2704.

[48] M. Schamel, C. Schopf, D. Linsler, S.T. Haag, L. Hofacker, C. Kappel, H.P. Strunk, G. Richter, The filamentary growth of metals, Int. J. Mat. Res. 102 (2011) 828–836.

[49] A. Wohllebe, B. Holländer, S. Mesters, C. Dieker, G. Crecelius, W. Michelsen, S. Mantl, Surface diffusion of Fe and island growth of FeSi₂ on Si(111) surfaces, Thin Solid Films 287 (1996) 93–100.

[50] T. Isobe, H. Nakashima, K. Hashimoto, Diffusion coefficient of interstitial iron in silicon, Jpn. J. Appl. Phys. 28 (1989) 1282–1283.

[51] D. Bergner, Y. Khaddour, S. Lörx, DIMETA-88, diffusion in metals and alloys, in: F.J. Kedves, D.L. Beke (Eds.),Defect and Diffusion Forum 1989, pp. 66–69 , (1407).

[52] E.S. Buflington, K.I. Hirano, M. Cohen, Self diffusion in iron, Acta Met 9 (1961) 434–439.

[53] L. Ruch, D.R. Sain, H.L. Yeh, L.A. Girifalco, Analysis of diffusion in ferromagnets, J. Phys. Chem. Solids 37 (1976) 649–653.

[54] T.Y. Tan, U. Gösele, Point defects, diffusion, and precipitation, in: K.A. Jackson, W. Schrter (Eds.), Handbook of Semiconductor Technolgy, vol. 1, Wiley-VCH, Weiheim 2000, p. 231.

[55] A. Wawro, S. Suto, R. Czajka, A. Kasuya, Thermal reaction of iron with a Si(111) vicinal surface: surface ordering and growth of CsCl-type iron silicide, Phys. Rev. B 67 (2003), 195401.

[56] K.N. Tu, Selective growth of metal-rich silicide of near-noble metals, Appl. Phys. Lett. 27 (1975) 221–224.

[57] A.P. Sutton, R.W. Balluffi, Interfaces in Crystalline Materials, Oxford University Press, 1995.

[58] V. Ruth, J.P. Hirth, Kinetics of diffusion-controlled whisker growth, J. Chem. Phys. 41 (1964) 3139–3149.

[59] I.N. Stranski, R. Kaischew, Gleichgewichtsform und Wachstumsform der Kristalle, Ann. Physik 5. Folge 23 (1935) 330–338.